Soft Matter

# Poroelasticity of highly confined hydrogel films measured with a surface forces apparatus



| | |
|---|---|
| Journal: | *Soft Matter* |
| Manuscript ID | SM-COM-07-2020-001312.R1 |
| Article Type: | Communication |
| Date Submitted by the Author: | 15-Aug-2020 |
| Complete List of Authors: | Degen, George; University of California Santa Barbara, Department of Chemical Engineering<br>Chen, Jonathan; University of California Santa Barbara, Department of Chemical Engineering<br>Chau, Allison; University of California Santa Barbara, Materials<br>Månsson, Lisa; Chalmers University of Technology, Department of Applied Physics<br>Pitenis, Angela; University of California Santa Barbara, Materials |
| | |

COMMUNICATION

# Poroelasticity of highly confined hydrogel films measured with a surface forces apparatus

Received 00th January 20xx,
Accepted 00th January 20xx

DOI: 10.1039/x0xx00000x

George D. Degen,*[a] Jonathan Chen,[a] Allison L. Chau,[b] Lisa K. Månsson[c] and Angela A. Pitenis[b]

**The influence of poroelasticity on the contact mechanics of thin polyacrylamide films was investigated with a surface forces apparatus (SFA). A model based on a thin film approximation described compression forces for hydrated gels and polymer scaling theory explained the effects of gel dehydration. The results demonstrate that fluid flow dictates the apparent stiffness of highly confined poroelastic films.**

Hydrated biopolymer films coat surfaces throughout the human body and include the surface layers of articular cartilage (thickness 4-8 μm)[1–3] and the mucosal layers lining the endothelium (1-5 μm),[4] ocular surface (1-5 μm),[5] airways (7-70 μm),[6] and intestines (20-150 μm).[7] Because these materials can be difficult to study directly, synthetic hydrogels with matching water content and stiffness are often used as model systems. Hydrogels are also used for medical implants[8] and drug delivery.[9,10] Natural and synthetic hydrated networks often exhibit poroelasticity, where elasticity and fluid flow govern mechanical properties. For a poroelastic film compressed between impermeable surfaces, the effect of fluid flow is amplified when the width of the contact region is much larger than the film thickness.[11] Such confinement is particularly likely for thin films. Therefore, to better understand and mimic biological surfaces, it is important to study the poroelasticity of highly confined gel films.

Although the mechanical properties of hydrogels have been widely investigated,[12] most studies of hydrogel poroelasticity report relatively low levels of confinement. These studies typically involve a sphere of radius $R$ compressing a gel film of thickness $h$ to a depth $d$ and approximate contact radius $\sqrt{2Rd}$. Confinement in this geometry is described by the dimensionless number[13] $\alpha = \sqrt{Rd}/h$, proportional to the ratio of contact width to film thickness. Poroelasticity has been observed in hydrogels with low confinement ($\alpha \ll 1$),[14–17] and moderate confinement ($\alpha \approx 1$),[13,18] but few studies of highly confined ($\alpha \gg 1$) hydrogels have been reported.[19–21]

The surface forces apparatus (SFA) is often used to study highly confined films.[22] While early SFA experiments were limited to nanoscale films, developments in instrumentation and analysis[23–26] have enabled studies of microscale films of poroelastic biological materials. For example, poroelasticity was shown to influence the mechanical properties of sections of corneal tissue[27] (thickness 150-300 μm). Films of fibronectin[28] (10-20 μm) and cartilage[29] (8-12 μm) have also been studied, but the experimental designs minimized poroelastic effects. Despite these examples of SFA studies of poroelastic materials, microscale films of synthetic hydrogels have not previously been studied in an SFA.

We investigated the contact mechanics of highly confined hydrogel films using a surface forces apparatus. In each experiment, a swollen crosslinked polyacrylamide film (7.5 wt% PAAm, 0.3 wt% bisacrylamide) was established on a cylindrical silver-coated glass surface (Figure 1A, Figure S1). In the SFA, the film was compressed against a bare silver surface in a crossed cylinder geometry (Figure 1B), equivalent to a sphere compressing a flat gel. The film thickness $h$, compression depth $d$ and velocity $\mathrm{d}(d)/\mathrm{d}t$, and normal force $F$ were measured. The cylinder radii ($R$ = 2 cm) were much larger than the film thickness ($h$ = 1-70 μm), yielding a highly confined contact region ($\alpha$ = 10-40), with $\alpha$ calculated from $d$ at maximum compression. A schematic of the SFA is shown in Figure S2. Details of film preparation, distance/force measurements, and crossed cylinder geometry are included in the Supporting Information S1-3.

The gels were modeled as thin poroelastic films[19] where the normal force $F$ needed to compress a film to a depth $d$ is

$$F = \frac{\pi R d^2}{h}\left(E + \frac{\eta R \mathrm{d}(d)}{2k\ \mathrm{d}t}\right) \quad (1)$$

Here, $E$ and $k$ are the elastic modulus and permeability of the gel, $\eta$ is the dynamic viscosity of the fluid, $R$ is the radius of each cylindrical surface, and $\mathrm{d}(d)/\mathrm{d}t$ is the compression velocity. Compression forces were also approximated by the Winkler model,[30] adapted to include the influence of fluid flow:

$$F = \frac{\pi R d^2}{h} E_{\mathrm{eff}} = \frac{\pi R d^2}{h}(E + E_{\mathrm{flow}}) \quad (2)$$

where the effective modulus $E_{\mathrm{eff}}$ is the sum of the elastic modulus $E$ and the average contribution of fluid flow $E_{\mathrm{flow}}$. At equilibrium, $\mathrm{d}(d)/\mathrm{d}t$ = 0, $E_{\mathrm{flow}}$ = 0, and both equations give $F = \pi R E d^2/h$. Viscoelasticity was neglected because confinement makes the

[a] Department of Chemical Engineering, University of California, Santa Barbara, Santa Barbara, CA 93106, USA. E-mail: gdegen@ucsb.edu
[b] Materials Department, University of California, Santa Barbara, Santa Barbara, CA 93106, USA.
[c] Department of Physics, Chalmers University of Technology, SE-412 96 Gothenburg, Sweden

Electronic Supplementary Information (ESI) available. See
DOI: 10.1039/x0xx00000x

timescales of poroelasticity much longer than the timescales of viscoelasticity.[13]

The apparent stiffness of the hydrogel films depended on the compression velocity. Figure 2A shows plots of normal force $F$ vs. compression depth $d$ for a hydrogel film ($h$ = 11 μm, $\alpha$ = 10) compressed at different initial velocities $\mathrm{d}(d)/\mathrm{d}t|_{d=0}$ = 11, 28, and 61 nm/s. As velocity increased, larger forces were needed to reach a given compression depth and the pressure at maximum compression increased from $P_{avg}$ = 2 to 7 kPa. Velocity-dependent stiffness was also observed for thicker films (Figure S3).

The apparent stiffness also depended on the film thickness. Figure 2B shows plots of $F$ vs. $d$ for three films of different thicknesses ($h$ = 11, 32, and 68 μm), each compressed at the same initial compression velocity 28-30 nm/s to pressure $P_{avg}$ = 6 kPa. As thickness increased, confinement decreased from $\alpha$ = 14 to 5 and less force was needed to reach a given compression depth. We note that the repulsion at $d$ = 0 for the 32 μm film may have resulted from roughness due to swelling (Supporting Information S1).

Equation (1) accounted for the variations in apparent stiffness of the gels. To determine the elastic modulus $E$ and permeability $k$ for the equation, relaxation experiments were conducted. A hydrogel film ($h$ = 11 μm) was compressed to initial force $F_0$ and compression depth $d_0$, at which point the motor driving the cantilever spring suspending one surface was stopped, denoted time $t$ = 0. For $0 < t < \Delta t$, compression depth increased, and force decreased as $F = F_0 - K(d - d_0)$, where $K$ is the cantilever spring constant. Figure 2C shows plots of compression velocity $\mathrm{d}(d)/\mathrm{d}t$ vs. relaxation time $t$ for three consecutive relaxation periods ($\Delta t$ = 1, 5, and 20 min). During each period, compression velocity decreased. The surfaces eventually became nearly stationary, $\mathrm{d}(d)/\mathrm{d}t \approx 0$, at compression depth $d_\infty$ and force $F_\infty = F_0 - K(d_\infty - d_0)$. Equations (1) and (2) then reduce to $E = hF_\infty/\pi R d_\infty^2$, giving $E$ = 14.9 ± 0.7 kPa. The uncertainty corresponds to variations in $d_\infty$ with time, likely due to thermal drift (Figure S4). This value of $E$ is consistent with previous studies of polyacrylamide hydrogels of the same polymer and crosslinker concentrations. A colloidal probe compression study[31] found $E$ = 9 kPa; a bulk compression study[32] suggested $E \approx$ 22 kPa.[33]

The relaxation experiments also yielded the permeability $k$ of the gels. Fits for $k$ of Equation (1) to the three relaxations shown in Figure 2C were performed. The fits are shown as dashed and solid red curves in Figure 2C and yielded $k$ = 1.28 ± 0.01 nm$^2$, where the uncertainty corresponds to the standard deviation. Fits using the lower and upper bounds of $E$ (14.2 and 15.6 kPa, respectively) also gave $k$ varying by ± 0.01 nm$^2$. The fitted value of permeability is consistent with reported values[12] and a theoretical approximation ($k \approx$ 2 nm$^2$, Supporting Information S4).

The elastic modulus and permeability from the relaxation experiments were used to calculate hydrogel compression forces with Equation (1) (Supporting Information S5). To validate the model, calculated forces were compared to the data shown in Figure 2A-B. The film thickness used to calculate each compression was determined with a one-parameter fit of Equation (1) to the measured forces. Calculated forces are shown as black curves in Figure 2A-B and match the measured forces. This agreement supports the accuracy of $E$ and $k$ and justifies the use of the poroelastic model. Discrepancies between predicted and measured forces may result from surface roughness (Supporting Information S1) or, particularly for the thicker films, failure of the thin film assumption used to derive Equation 1 (Supporting Information S3).

As shown above, the film thickness, elastic modulus, and permeability contribute to the apparent stiffness of highly confined hydrogel films. These parameters are related to the water content of the gel. To explore the influence of hydration on hydrogel poroelasticity, ethanol solutions were used to dehydrate a gel film. The film was initially immersed in a capillary meniscus of pure water which was exchanged with solutions of increasing ethanol fraction $x_{EtOH}$. Because ethanol is a poor solvent for polyacrylamide,[34] increased $x_{EtOH}$ corresponded to decreased hydration of the gel. Figure 3A shows compression forces measured at each ethanol fraction. As $x_{EtOH}$ increased, more force was needed to reach a given compression depth. This increase in apparent stiffness is consistent with previously reported stiffening of hydrogels in ethanol.[14] For $x_{EtOH} < 1$, repeated compressions showed no hysteresis, while for $x_{EtOH}$ = 1, the film thinned and stiffened over repeated compressions (Figure S5). The data for $x_{EtOH}$ = 1 in Figure 3A correspond to the last compression of the film.

The increase in apparent stiffness of the film with increasing ethanol fraction was partially attributed to a change in film thickness. The forces shown in Figure 3A were fit with Equation (2) for $h$ and $E_{eff}$. The fits appear as curves in Figure 3A; the inset shows the fitted $h$ vs. $x_{EtOH}$. As $x_{EtOH}$ increased, $h$ decreased, consistent with a previous report of deswelling of polyacrylamide hydrogels in ethanol solutions.[35] When compressing a soft film on a rigid substrate, more force is needed to reach a given compression depth for a thin film than a thick film, shown by $h$ in the denominator of Equations (1) and (2). Therefore, the decrease in film thickness with increasing ethanol fraction was expected to increase the apparent stiffness of the gel.

However, the increase in apparent stiffness with increasing ethanol fraction cannot be entirely attributed to the decrease in film thickness. Figure 3B shows the effective modulus $E_{eff}$ from the fits (black circles). As $x_{EtOH}$ increased, $E_{eff}$ increased. If the decrease in $h$ entirely accounted for the stiffening, then $E_{eff}$ would be independent of $x_{EtOH}$. Since $E_{eff}$ increased with $x_{EtOH}$, changes in film properties likely contributed to the increase in apparent stiffness.

Polymer scaling theory accounts for the increase in effective modulus. Scaling theory[36] relates the elastic modulus of a swollen crosslinked gel in a good solvent to the polymer concentration $c$ as $E \propto c^{2.25}$. For a gel film of thickness $h_0$ and polymer concentration $c_0$ collapsing to thickness $h$ and concentration $c$, conservation of mass requires that $c_0 h_0 = ch$. This expression assumes that the gel shrinks in only one dimension due to the surface preparation, justified by the uniform profile after swelling (Figure S1) and the agreement between swelling ratios calculated for thin films and macroscopic gels (Figure S6). The scaled elastic modulus at each ethanol fraction can thus be calculated as $E_{scaled} = E_0(h_0/h)^{2.25}$ (Figure 3B, orange circles), where $h_0$ (11 μm) and $E_0$ (15 kPa) are the thickness and elastic modulus of the gel in pure water ($x_{EtOH}$ = 0) and $h$ is the film thickness at each ethanol fraction. Because $h$ monotonically decreased with increasing $x_{EtOH}$, $E_{scaled}$ increased. For $x_{EtOH}$ = 1, the scaled elastic modulus exceeded the effective modulus ($E_{scaled} = E_{eff}$). This result is not physically meaningful because neither $E$ nor $E_{flow}$ may exceed $E_{eff}$ in Equation (2). The inaccuracy likely occurs because the scaling relationship assumes a good solvent, but ethanol is a poor solvent for polyacrylamide.[34] Therefore, the relationship is expected to fail at high ethanol concentrations. Linear interpolation gives $E_{scaled} > E_{eff}$ for $x_{EtOH} > 0.42$ (Figure 3B, right of dotted line), suggesting that for $x_{EtOH} > 0.42$, the scaling relationship fails and the apparent stiffness results entirely from elasticity ($E = E_{eff}$).

The values of $E_{scaled}$ and $E_{eff}$ were used to calculate the average contribution of fluid flow to the effective modulus. Taking $E = E_{scaled}$ in Equation (2) gives $E_{flow} = E_{eff} - E_{scaled}$ for $x_{EtOH} < 0.42$. For $x_{EtOH} > 0.42$, $E_{flow}$ = 0 because $E = E_{eff}$ as discussed above. The value of $E_{flow}$ at each ethanol fraction is shown in Figure 3B (blue circles). The non-monotonic dependence of $E_{flow}$ on $x_{EtOH}$ likely results from a

 

combination of three factors: i) scaling theory[36] predicts that permeability of a swollen gel decreases with increasing polymer concentration as $k \propto c^{-1.5}$; decreased permeability increases $E_{flow}$. ii) The viscosity of an ethanol/water solution changes non-monotonically with ethanol fraction (Figure S7); increased viscosity increases $E_{flow}$. iii) The changes in elastic modulus, permeability, and solution viscosity influence the compression velocity d($d$)/d$t$; increased velocity increases $E_{flow}$. Calculation of $E_{flow}$ is further complicated by the uncertainty in $E$ as the gel collapses and the assumption of a good solvent used to derive the scaling relationship is increasingly violated.

Comparing $E_{scaled}$ to $E_{flow}$ reveals the relative contributions of elasticity and fluid flow to the apparent stiffness. Linear interpolation suggests that for $x_{EtOH} < 0.3$, fluid flow provides a greater contribution to $E_{eff}$ than elasticity ($E_{flow} > E_{scaled}$), while for $x_{EtOH} > 0.3$, elasticity contributes more than fluid flow ($E_{scaled} > E_{flow}$). As discussed above, for $x_{EtOH} > 0.42$, $E_{scaled}$ is not physically meaningful, and instead $E = E_{eff}$ and $E_{flow} = 0$. However, it is likely that polymer scaling fails somewhat before $x_{EtOH} = 0.42$, possibly near $x_{EtOH} = 0.3$ where $E_{scaled}$ exceeds $E_{flow}$. Nevertheless, the results indicate that fluid flow is predominantly responsible for the apparent stiffness of the hydrated gels. We suggest that fluid flow may similarly influence the mechanical properties of thin gel layers in the body, especially since the strain rates applied here ($10^{-4}$-$10^{-2}$ $s^{-1}$) are low compared to the strain rates relevant to articular cartilage[37] ($10^{-5}$-$10^{3}$ $s^{-1}$) and tissues in the heart and lungs[38] ($10^{-1}$-$10^{1}$). Relatively large strain rates likely also occur in the corneal epithelium during eye rubbing.[39] These biological strain rates are expected to further amplify the effect of fluid flow on the mechanical properties of confined poroelastic films.

In summary, we used a surface forces apparatus to study the contact mechanics of highly confined polyacrylamide films. The elastic modulus and permeability were measured and used to calculate compression forces for different film thicknesses and compression velocities. Polymer scaling theory explained film stiffening with decreasing hydration and showed that fluid flow dictates the contact mechanics of highly confined hydrated gels. We anticipate that our work will enable future studies of thin hydrogel films for improved medical implants and drug delivery systems.

## Conflicts of interest

There are no conflicts to declare.

## Acknowledgements

The authors thank Professor Robert McMeeking for helpful derivations and discussions. G.D.D. and A.L.C. were supported by the National Science Foundation Graduate Research Fellowship Program under Grant No. 1650114. This work was supported by the Materials Research Science and Engineering Center (MRSEC) at UC Santa Barbara through NSF Grant No. DMR-1720256 (IRG-3).

## References

1 R. Teshima, T. Otsuka, N. Takasu, N. Yamagata and K. Yamamoto, *J. Bone Jt. Surg. - Ser. B*, 1995, **77**, 460.
2 R. Crockett, S. Roos, P. Rossbach, C. Dora, W. Born and H. Troxler, *Tribol. Lett.*, 2005, **19**, 311.
3 R. Fujioka, T. Aoyama and T. Takakuwa, *Osteoarthr. Cartil.*, 2013, **21**, 1092.
4 S. Reitsma, D. W. Slaaf, H. Vink, M. A. M. J. Van Zandvoort and M. G. A. Oude Egbrink, *Pflugers Arch. Eur. J. Physiol.*, 2007, **454**, 345.
5 R. R. Hodges and D. A. Dartt, *Exp. Eye Res.*, 2013, **117**, 62.
6 C. L. Hattrup and S. J. Gendler, *Annu. Rev. Physiol.*, 2008, **70**, 431.
7 C. Atuma, V. Strugala, A. Allen and L. Holm, *Am. J. Physiol. - Gastrointest. Liver Physiol.*, 2001, **280**, G922.
8 E. Caló and V. V. Khutoryanskiy, *Eur. Polym. J.*, 2015, **65**, 252.
9 N. A. Peppas, P. Bures, W. Leobandung and H. Ichikawa, *Eur. J. Pharm. Biopharm.*, 2000, **50**, 27.
10 C. M. Kirschner and K. S. Anseth, *Acta Mater.*, 2013, **61**, 931.
11 M. Galli and M. L. Oyen, *Appl. Phys. Lett.*, 2008, **93**, 31911.
12 M. L. Oyen, *Int. Mater. Rev.*, 2014, **59**, 44.
13 E. P. Chan, Y. Hu, P. M. Johnson, Z. Suo and C. M. Stafford, *Soft Matter*, 2012, **8**, 1492.
14 M. Galli, K. S. C. Comley, T. A. V. Shean and M. L. Oyen, *J. Mater. Res.*, 2009, **24**, 973.
15 Y. Hu, X. Zhao, J. J. Vlassak and Z. Suo, *Appl. Phys. Lett.*, 2010, **96**, 121904.
16 E. R. Reale and A. C. Dunn, *Soft Matter*, 2017, **13**, 428.
17 M. H. Esteki, A. A. Alemrajabi, C. M. Hall, G. K. Sheridan, M. Azadi and E. Moeendarbary, *Acta Biomater.*, 2020, **102**, 138.
18 Z. I. Kalcioglu, R. Mahmoodian, Y. Hu, Z. Suo and K. J. Van Vliet, *Soft Matter*, 2012, **8**, 3393.
19 J. Delavoipière, Y. Tran, E. Verneuil and A. Chateauminois, *Soft Matter*, 2016, **12**, 8049.
20 J. Delavoipière, Y. Tran, E. Verneuil, B. Heurtefeu, C. Y. Hui and A. Chateauminois, *Langmuir*, 2018, **34**, 9617.
21 L. Ciapa, J. Delavoipière, Y. Tran, E. Verneuil and A. Chateauminois, *Soft Matter*, 2020.
22 L. Xiang, J. Zhang, L. Gong and H. Zeng, *Soft Matter*, 2020, **16**, 6697.
23 J. Israelachvili, Y. Min, M. Akbulut, A. Alig, G. Carver, W. Greene, K. Kristiansen, E. Meyer, N. Pesika, K. Rosenberg and H. Zeng, *Reports Prog. Phys.*, 2010, **73**, 036601.
24 M. Heuberger, *Rev. Sci. Instrum.*, 2001, **72**, 1700.
25 K. A. Schwenzfeier, A. Erbe, P. Bilotto, M. Lengauer, C. Merola, H. W. Cheng, L. L. E. Mears and M. Valtiner, *Rev. Sci. Instrum.*, 2019, **90**, 043908.
26 K. Kristiansen, S. H. Donaldson, Z. J. Berkson, J. Scott, R. Su, X. Banquy, D. W. Lee, H. B. De Aguiar, J. D. McGraw, G. D. Degen and J. N. Israelachvili, *Langmuir*, 2019, **35**, 15500.
27 T. Shoaib, C. Yuh, M. A. Wimmer, T. M. Schmid and R. M. Espinosa-Marzal, *Biomater. Sci.*, 2020.
28 K. Wang, R. C. Andresen Eguiluz, F. Wu, B. R. Seo, C. Fischbach and D. Gourdon, *Biomaterials*, 2015, **54**, 63.
29 B. Zappone, N. J. Patil, M. Lombardo and G. Lombardo, *PLoS One*, 2018, **13**, e0197779.
30 K. L. Johnson, *Contact Mechanics*; Cambridge University Press: Cambridge, 1985.
31 Y. A. Meier, K. Zhang, N. D. Spencer and R. Simic, *Langmuir*, 2019, **35**, 15805.
32 K. D. Schulze, S. M. Hart, S. L. Marshall, C. S. O'Bryan, J. M.

Urueña, A. A. Pitenis, W. G. Sawyer and T. E. Angelini, *Biotribology*, 2017, **11**, 3.
33 Ref. 32 reports a plane strain modulus $E^* = E/(1 - \nu^2)$ corresponding to $E \approx 22$ kPa, assuming Poisson's ratio $\nu = 0.5$.
34 S. Wu and R. A. Shanks, *J. Appl. Polym. Sci.*, 2004, **93**, 1493.
35 J. Erfkamp, M. Guenther and G. Gerlach, *J. Sensors Sens. Syst.*, 2018, **7**, 219.
36 P. G. de Gennes, *Scaling Concepts in Polymer Physics*; Cornell University Press: Ithaca, NY, 1979.
37 A. Oloyede, R. Flachsmann and N. D. Broom, *Connect. Tissue Res.*, 1992, **27**, 211.
38 E. Moeendarbary, L. Valon, M. Fritzsche, A. R. Harris, D. A. Moulding, A. J. Thrasher, E. Stride, L. Mahadevan and G. T. Charras, *Nat. Mater.*, 2013, **12**, 253.
39 S. Masterton and M. Ahearne, *Exp. Eye Res.*, 2018, **177**, 122.

 

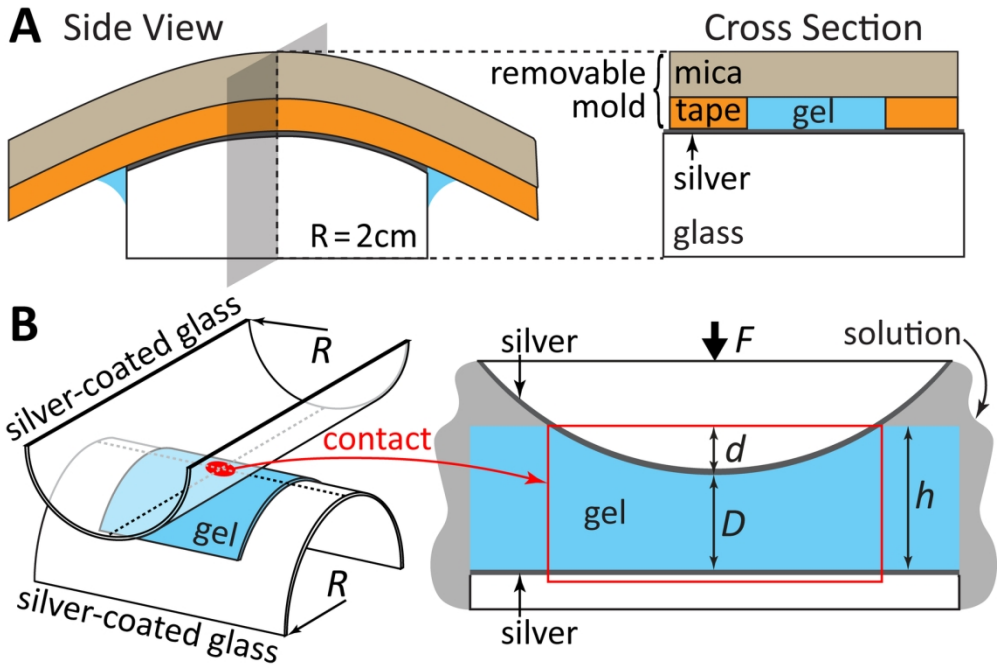


**Fig. 1** (A) Casting a hydrogel film on a cylindrical silver-coated glass surface. (B) Crossed cylinder configuration and schematic of the contact region for a gel film of thickness *h* under applied force *F*, resulting in surface separation *D* and compression depth *d*.

77x52mm (600 x 600 DPI)

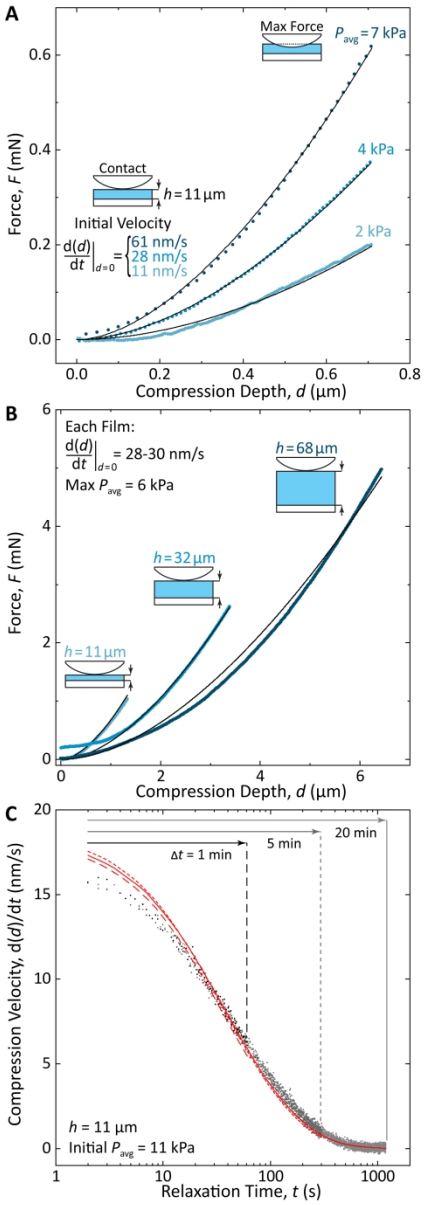


**Fig. 2** (A) Normal force $F$ vs. compression depth $d$ for a hydrogel film compressed at different initial velocities $d(d)/dt|_{d=0}$. (B) $F$ vs. $d$ for compressions of films of different thicknesses. Curves in (A) and (B) were calculated using Equation (1). (C) Compression velocity $d(d)/dt$ vs. relaxation time $t$ for sequential relaxations ($\Delta t$ = 1, 5, and 20 min). Dashed and solid red curves show fits of Equation (1) for permeability $k$.

77x223mm (600 x 600 DPI)

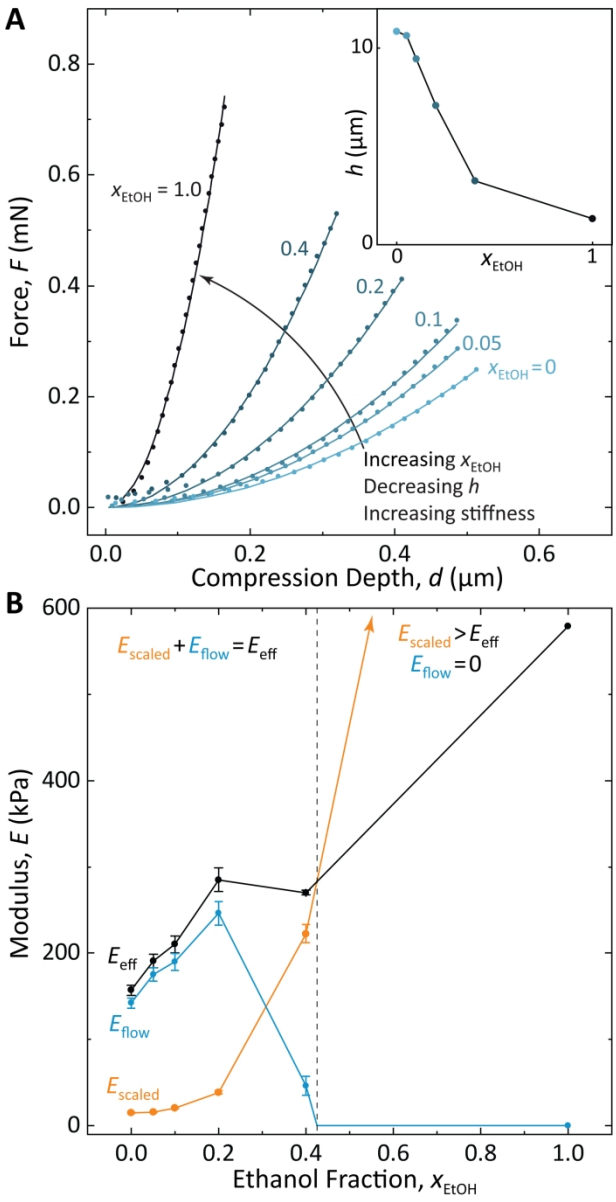


**Fig. 3** (A) $F$ vs. $d$ for a gel film in a solution of increasing ethanol fraction $x_{EtOH}$. Curves show fits of Equation (2). Inset: Film thickness $h$ vs. $x_{EtOH}$. (B) Effective modulus $E_{eff}$ (black circles), scaled elastic modulus $E_{scaled}$ (orange circles), and contribution of fluid flow $E_{flow}$ (blue circles) vs. $x_{EtOH}$. Dotted line shows the ethanol fraction at which $E_{scaled}$ exceeds $E_{eff}$. Error bars correspond to the standard deviation for $E_{eff}$, the scaled uncertainty in the measured elastic modulus in water for $E_{scaled}$, and the square root of the sum of squared errors of $E_{eff}$ and $E_{scaled}$ for $E_{flow}$.

76x150mm (600 x 600 DPI)

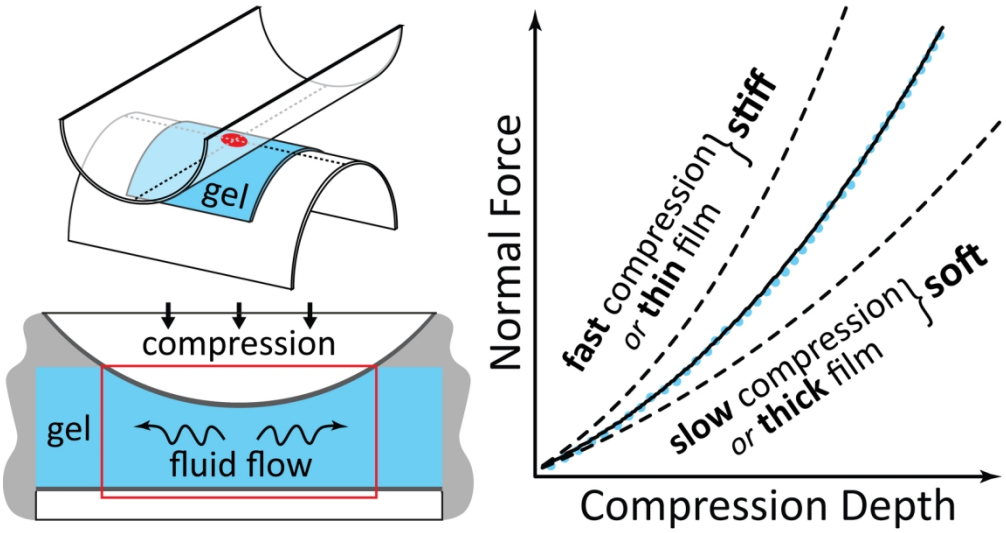


74x39mm (600 x 600 DPI)